# Satellite-Based Probabilistic Assessment of Soil Moisture Using C-Band Quad-Polarized RISAT1 Data

Manali Pal, Rajib Maity, Mayank Suman, Sarit Kumar Das, Parul Patel, and Hari Shanker Srivastava

***Abstract*— This paper attempts to probabilistically estimate the surface soil moisture content (SMC) by using the synthetic aperture radar data provided by radar imaging satellite1. The novelty of this paper lies in: 1) developing a combined index to understand the role of all the backscattering coefficients with different polarization and soil texture information in influencing the SMC; 2) using normalized incidence angles, which enables the model to be applicable for different incidence angles; and 3) determination of uncertainty range of the estimated SMC. The dimensionality problem, which is frequently observed in the multivariate analysis, is reduced in the development of the combined index by the use of supervised principal component analysis (SPCA). The SPCA also ensures the maximum attainable association between the developed combined index and surface SMC above wilting point (WP). The association between the combined index and the surface SMC above WP is modeled through joint probability distribution by using the Frank copula. The model is developed and validated with the field soil moisture values over 334 monitoring points within the study area. The outcomes obtained by applying the proposed model indicate an encouraging potential of the model to be applied for bareland and vegetated land (<30 cm height).**

***Index Terms*— Backscattering coefficients, copula, radar imaging satellite1 (RISAT1), supervised principal component analysis (SPCA).**

## I. Introduction

PRECISE details on spatio-temporal distribution of surface soil moisture content (SMC) have pronounced significance in many hydrological applications, such as predicting flood, forecasting the rainfall events, weather prediction, irrigation scheduling, management of water resource in the course of dry seasons, and so on [1]. In recent times, there has been an increasing importance in using microwave active remote sensing for surface SMC estimation, because of its all-weather [2], and day and night characteristics [3]. The use of synthetic aperture radar (SAR) in microwave active remote sensing is highly potential for catchment-scale applications due to very high spatial resolution (∼10–20 m) [3] both for vegetated and bare soil surface [4].

Despite an intensive study for soil moisture retrieval from SAR data for last two decades, one key drawback of SAR sensors is that their signal is subjective to SMC along with the land use land cover (LULC) and the surface roughness conditions. Consequently, the retrieval of SMC from SAR data becomes an alleged "ill-posed" problem, where amalgamation of various soil characteristics (SMC, vegetation, and roughness) can yield the identical SAR signal [3]. The primary complexity in inverting SMC using backscattering models for a natural surface is the incapability in precise illustration of the roughness of the natural soil surfaces [5]–[11]. The change detection approach is an effective method to take care of the uncertainty introduced by vegetation and roughness conditions on the field. In this approach, it is assumed that the average roughness characteristics and vegetation cover remain unaltered between successive satellite image acquisitions, whereas surface SMC variations mainly affect the backscattering signals [12]–[17]. Although the change detection approach can effectively represent the influence of surface roughness and low vegetation cover to a certain degree, the key restraint is the requirement of adequate SAR acquisitions to ensure the assumption of the consistency of surface roughness and LULC conditions among the different acquisitions. The development of single acquisition SMC retrieval process based on the inversion of physical-based forward electromagnetic models is a substantial alternative of the change-detection-based approaches [18]–[21]. However, the derived relationships presented by these empirical models are not usually transferrable [18]. The use of numerical backscattering models, such as the method of moments [22], finite-element method, and so on, is inhibited due to deficiency in advanced and faster computational resources [23]. In addition, the inversion of SMC from the analytical backscattering models, such as integral equation model [24], geometric optical model, small perturbation method [2], and so on, is difficult and erroneous due to incorrect representation of soil roughness [11]. Moreover, these are effective only for bare or thinly vegetated soil surfaces, which is an essential inadequacy

Manuscript received April 27, 2016; revised September 9, 2016; accepted October 17, 2016. Date of publication November 22, 2016; date of current version February 23, 2017. This work was supported by the Space Application Centre (SAC), Indian Space Research Organization under Grant IIT/SRIC/CE/PMA/2013-14/5.

M. Pal and M. Suman are with the School of Water Resources, IIT Kharagpur, Kharagpur 721302, India (e-mail: manalipal000@gmail.com; mayanksuman@protonmail.com).

R. Maity is with the Department of Civil Engineering, IIT Kharagpur, Kharagpur 721302, India, and also with the Karlsruhe Institute of Technology, Campus Alpin-IMK-IFU, Garmisch-Partenkirchen, Germany, (e-mail: rajib@civil.iitkgp.ernet.in; rajibmaity@gmail.com).

S. K. Das is with IIT Roorkee, Roorkee 247667, India (e-mail: saritkd81@gmail.com).

P. Patel is with the Space Applications Centre, Indian Space Research Organization, Ahmedabad 380015, India (e-mail: parul_isro@yahoo.com; parul@sac.isro.gov.in).

H. S. Srivastava is with the Agriculture and Soils Department, Indian Institute of Remote Sensing, Indian Space Research Organization, Dehradun 248001, India (e-mail: hari.isro@gmail.com).

Color versions of one or more of the figures in this paper are available online at http://ieeexplore.ieee.org.

Digital Object Identifier 10.1109/TGRS.2016.2623378

0196-2892 © 2016 IEEE. Personal use is permitted, but republication/redistribution requires IEEE permission.
See http://www.ieee.org/publications_standards/publications/rights/index.html for more information.

of these models for soil moisture retrieval. Determination of vegetation parameters, which are of utmost importance to differentiate the influence of vegetation on radar coefficients from soil, is difficult as they vary with incidence angle, wavelength, phenology, and so on. [25]. Presently, most studies on soil moisture retrieval from vegetated surfaces take place in an agricultural background, which involves considerable work to be done to conclude the vegetation impacts from natural vegetation and forests. Therefore, the lacunas of the above-mentioned studies clearly call attention to the potential of developing a model for dealing with the retrieval of fine-scale and near-real-time SMC products in a wide variety of land surface conditions from SAR remote sensing data. The existing literature also suggests the presence of uncertainty due to speckle, inappropriate surface roughness characterization, and inversion techniques, in the estimated soil moisture obtained from even the latest established methods [23]. While this uncertainty can never be brought down to zero, its quantification can be of tremendous use to better parameterization of soil moisture retrieval models when field sampling is not possible.

Soil moisture, identified as an essential climate variable by the United Nations Framework Convention on Climate Change, plays an important role for the environment and climate system through atmospheric feedbacks [26]. Thus, the soil moisture maps, having information at a very fine resolution, are of great importance in climate modeling as well as hydrological and agricultural modeling. In this paper, artificial neural network was used to prepare soil moisture map by using Sentinel-1 data [27]. The proposed approach is computationally challenging, since the algorithm should be able to process operationally in near-real-time and conveying the product to the global monitoring for environment and security services within 3 h of the observations. In addition, the algorithm needs the specific information about the vegetation in terms of NDVI to be applied in a global scenario. In the agenda of the European Space Agency's Water Cycle Multimission Observation Strategy and Climate Change Initiative projects, a global surface soil moisture map of daily scale is developed for the period 1979–2010 using two active (European Remote Sensing Satellite Active Microwave Instrument (ERS AMI), and Advanced Scatterometer (ASCAT) and four passive (Scanning Multi-channel Microwave Radiometer (SMMR), Special Sensor Microwave Imager (SSM/I), Tropical Rainfall Measuring Mission (TRMM) Microwave Imager (TMI), and Advanced Microwave Scanning Radiometer (AMSR-E) microwave remote sensing data, but the product is having a coarse spatial resolution (around 50 km) and low Spearman correlation coefficient (CC) (0.46) with the *in situ* observations [28], which restricts the extensive use of the product in climate, hydrological, and agricultural studies. Therefore, from the above-mentioned discussion, it can be concluded that the development of a nonsite specific, fine resolution soil moisture map will be of much importance in various field of studies.

The plants are unable to excerpt water below the wilting point (WP) which in turn affects the agricultural applications as well as the hydrological modeling, since the fact also influences the evapotranspiration. Thus, it indirectly influences the complete hydrological cycle along with the atmospheric circulations. Srivastava *et al*. [29] showed that the use of water available to plant per unit volume of soil above WP provides the better CC and lesser error. Therefore, the estimation of the SMC extracted by the plants and above WP is explored in this paper. The water that is essentially available to the plant is the difference between the observed SMC and the WP, i.e., the moisture at 15 bar suction pressure. The detail description of the computation of SMC at 15 bar is presented in the Appendix. Thus, the SMC mentioned in this paper refers to the SMC above the WP or available SMC hereafter.

TABLE I
DESCRIPTION OF SATELLITE IMAGE

| Date of passing | Incidence Angle | Scene Centre Lat | Scene Centre Lon |
|---|---|---|---|
| 25-OCT-2014 | 14.25039 | 22.194216 | 87.307328 |
| 27-OCT-2014 | 27.03315 | 22.190772 | 87.345272 |

Indian Space Research Organization has launched radar imaging satellite1 (RISAT1), on April 26, 2012. It uses a multimode SAR at C-band (5.35 GHz) from a sun-synchronous orbit at a nominal altitude of 536 km. The spatial and temporal resolutions of the satellite are 3–50 m and 25 days, respectively. It consists of five operational modes and four polarization modes. The improved spatial and temporal sampling due to the use of C-band can be effectively utilized to retrieve information about surface SMC.

The overall objective of this paper is to estimate the surface soil moisture above WP using data obtained from RISAT1. The research questions to be addressed in this paper are as follows—Is it possible to beneficially utilize the quad-polarized data in order to develop a stand-alone approach for soil moisture retrieval? Is it possible to consider incident angle normalization in such a method in order to make the model robust with respect to incident angle, so that a spatial map can be developed with the images having different incident angle? Is it possible to develop such a method avoiding the requirement of on-ground information on LULC and surface roughness at least for some LULC depending on the penetration depth of microwave remote sensing? Is it possible to quantify the uncertainty associated with the surface SMC estimation?

## II. STUDY AREA AND FIELD MEASUREMENTS

The study area of this paper is defined by the boundaries of the satellite images acquired. The SAR backscattering coefficient for RISAT1 is obtained for study area on Oct 25, 2014 and Oct 27, 2014. The image on Oct 25 is enclosed by the following four coordinates, 22° 1'50.37"N × 87° 13'51.26"E; 22° 4'6.1104"N × 87° 26'9.57"E; 22° 21'21.94"N × 87° 22'30.62"E; 22° 19'6.77"N × 87° 10'14.06"E. Similarly, the image on Oct 27 is enclosed by the following four coordinates, 22° 4'16.84"N × 87° 29'45.13"E; 22° 1'26.3892"N × 87° 16'2.86"E; 22° 18'39.04"N × 87° 11'53.35"E; 22° 21'30.2364"N × 87° 25'39.39"E. The RISAT1 data are procured from the National Remote Sensing Center (NRSC), Hyderabad, India, in Fine Resolution Stripmap Mode 2 (FRS-2)

TABLE II
STUDY AREA DESCRIPTION

| Type of LULC | Sampling Points | v/v SMC range | %Gravel | %Sand | %Silt | %Clay |
|---|---|---|---|---|---|---|
| Bare | 55 | 1.48-39.19 | 0-20.34 | 37.16-67.07 | 17.54-53.12 | 3.87-15.74 |
| Vegetation | 320 | 2.14-73.59 | 0-20.34 | 7.62-73.01 | 17.54-65.74 | 0.46-26.61 |

mode. Table I represents the specifications of the procured satellite image. Within the extent of this image, the soil samples within the top 5 cm of the surface are collected from 334 monitoring points.

It is worthwhile to mention two points here. First, the satellite passed the study area at 5:00 P.M. (IST). In order to assure the accuracy of the ground truth, the soil samples were collected within $\pm 1$ h of satellite visit. Almost no change in SMC, owing to soil humidity change, between time of satellite passing and the time of soil sample collection is assured through collection the soil sample as close to the time of satellite passing as possible. Second, the penetration depth of RISAT1 is not more than 30 cm of vegetation height. It restricts the model to be applied only for less than 30 cm vegetation height. Thus, the soil samples were collected from barelands and vegetated lands having $<30$ cm vegetation height.

The collected soil samples are analyzed in the laboratory to determine the volumetric SMC and the soil texture information. The moisture contents of the soil samples in weight fraction are determined by the Gravimetric Method (IS:2720, Part-2, 1973). Therefore, to calculate the volumetric SMC, the specific gravity and the porosity of the collected soil samples are determined following the Indian Standard IS:2720 [30]. The particle size distribution and the sand, silt, and clay contents of the soil samples were determined by sieve analysis and hydrometer analysis [31].

A brief description of the experimental result is given in Table II. The soil composition of the study area is obtained from the experimental results. It is observed that the gravel, sand, silt, and clay amount varies from 0.026%–20.338%, 7.26%–73.010%, 1.080%–65.744%, and 0.202%–26.610% respectively. Therefore, it can be said that the soil texture of the study area is mainly sandy and silty.

## III. METHODOLOGY

### A. Satellite Image Acquisition and Processing

The FRS-2 mode images are available in quad polarization mode. The polarization of incident radar signal is either horizontal ($H$) or vertical ($V$), and the backscatter is also received in these polarization. Thus, the outcome is either co-polarized ($HH$ or $VV$) or cross-polarized ($HV$ or $VH$) backscattering coefficient, which is denoted by $\sigma_0$. The quantity of energy backscattered from a natural surface is subjected to the radar configuration, soil characteristics, and vegetation characteristics. The quad-polarized (all four polarizations, i.e., $HH$, $HV$, $VH$, and $VV$) SAR data are procured from NRSC for the two images mentioned earlier. For each image, the digital numbers supplied by NRSC, the effect of the "speckle" due to multiple within-pixel scattering objects is removed. The speckle filtered digital numbers ($DN_p$) are converted into a backscattering coefficients expressed in decibel (dB) using the SAR calibration coefficient for each linear polarization using the equation from the RISAT1 data products format suggested by Space Application Center [32] and represented as the following:

$$\sigma_0 = 20\log_{10}(DN_p) - K_{\mathrm{dB}} + 10\log_{10}\frac{\sin i_p}{\sin i_c} \qquad (1)$$

where $\sigma_0$ is the radar backscatter coefficient in dB, $DN_p$ is the digital number for the pixel $p$, $K_{\mathrm{dB}}$ is the calibration constant, $i_p$ is the incidence angle at pixel position $p$, and $i_c$ is the incidence angle at scene center. Incidence angle for the center of $32 \times 32$ pixel block is provided with the image. Therefore, the incidence angle at any pixel position $p$ is computed by bicubic interpolation from the neighboring grid points.

### B. Incidence Angle Normalization

The previous studies using SAR data have presented the prospective of radar signals to estimate surface SMC with a single incidence-angle data and a linear relationship. Thus, for the same surface roughness and polarization values, the linear relationship between the radar backscattering values and the surface SMC needs the same incidence angle for each image acquisition. In that case, the temporal resolution is very low (e.g., 35 days for European Remote Sensing satellites). Such coarse temporal resolution of data is not sufficient for hydrologic studies. On the other hand, the diversity in incidence angles allows frequent image acquisition. In our case, the RISAT1 data correspond to two different incidence angles, each for two different dates. Since the backscattering values highly vary with the different incidence angles of the sensor, it is not possible to combine the backscattering values of the two dates to investigate the association between the backscattering values and the surface SMC. Hence, to study the sensitivity of the backscattering values of the two different dates to the surface SMC, the measurements should be normalized to a reference incidence angle. This paper follows the methodology proposed by Zribi *et al.* [33], who prepared a library with the backscattering values and the incidence angles corresponding to large ranges of surface roughness conditions. The root-mean-square (rms) height of surface roughness ($s$) varies from 0.5 to 2 cm and the radar signal is nearly saturated for $s > 2$ cm. The correlation function shape can be directly computed from the rms height. Using the numerical approach described by Fung and Chen [34], different surfaces characterized by these three parameters are simulated. In the simulation, three values of the correlation length are considered representing a large variation interval ($l = 3$ cm, $l = 6$ cm, and $l = 9$ cm). The backscattering coefficient is estimated for each surface roughness for a wide variety of incidence angle. The simulated library of the backscattering coefficients for extensive ranges of surface roughness parameter allows the proposed simulation model to utilize the multi-incidence angle data of different dates.

In this paper, the library realization prepared by Zribi *et al.* [33] is used to normalize the backscattering

values obtained from RISAT1 to a reference angle of 30°. The incidence angles at each pixel $p$ were normalized to the reference angle.

### C. Supervised Principal Component Analysis

Unlike principal component analysis (PCA), the supervised PCA (SPCA) is able to yield the principal components in order of its association with a target variable [35]. Thus, the first component is expected to possess maximum association with the target variable. The approach of SPCA utilizes the Hilbert–Schmidt independence criterion (HSIC) to develop the principle components, which is based on an orthogonal transformation of the input matrix [36]. In this paper, SPCA is adopted for dimensionality reduction of the inputs and to develop a combined index for the estimation of the volumetric surface SMC. It is explained briefly as follows.

Suppose, a set of $n$ observed data points each comprising of $p$ variables form the input matrix, $X$ of $p \times n$ dimension and $Y$ is the $1 \times n$ dimensional data matrix of the target output variable. The SPCA technique deals with the problem of finding the subspace $U^T X$ to maximize the association between the output variable $Y$ and the projected input matrix $U^T X$, where $U$ is an orthogonal projection matrix of size $p \times 1$. In order to estimate the association between the $U^T X$ and the output $Y$, the HSIC is used. As stated by HSIC, the degree of dependence between two random variables, $X$ and $Y$, is related with their reproducing kernel Hilbert space (RKHS) [36]. The RKHS is a pointwise assessment a complete, (probably) linear space of infinite dimension provided with an inner product [37]. The HSIC states, $X$ and $Y$, are independent if and only if any bounded continuous functions of the considered random variables are not correlated with each other [35]. For a given finite number of observations, the HSIC should be estimated to make it a practical criterion for testing the independence. Therefore, an empirical estimation of HSIC for $n$ number of independent observations can be represented by the following equation:

$$HSIC(Z, F, G) := (n-1)^{-2}\mathrm{tr}(KHLH) \tag{2}$$

where $Z := \{(x_1, y_1), \ldots, (x_n, y_n)\} \subseteq X \times Y$ is the series of independent and identically distributed samples; $F$ and $G$ are defined as the separable RKHS consisting of all likely continuous bounded real-valued functions of $x$ from $X$ to $\Re$ and $y$ from $Y$ to $\Re$, respectively; the kernels are $H, K$, $L \in \Re^{n \times n}$, $K_{ij} := k(x_i, x_j)$, $L_{ij} := l(y_i, y_j)$, and $H_{ij} := I - n^{-1}ee^T$ where $I$ is an $n \times n$ dimensional unit vector and the 1-D vector $e$ consisting of all ones and length $n$ and tr(...) refers to the "trace" of the matrix (...). For obtaining the principal component which has the maximum association with the output variable $Y$, the trace of the reduced matrix $[KHLH]$ is maximized, where $K$ is a kernel of $U^T X$ and $L$ is a kernel of $Y$. Conforming to the cyclic permutation of trace of a product, if either of $K$ or $L$ is already centered, for example $L$, then $HLH = L$. Therefore, the objective function, $\mathrm{tr}(KL)$ which does not consist of the centering matrix $H$ any longer, can be used. Likewise, if $HKH = K$, then $\mathrm{tr}(KHLH)$ can be revised as $\mathrm{tr}(HKHL)$, which can be described as follows:

$$\mathrm{tr}(HKHL) = \mathrm{tr}(HX^T UU^T XHL) \tag{3}$$

where $K$ and $L$ are stated as $[X^T UU^T X]$ and $[Y^T Y]$, respectively. Equation (3) can also be rearranged as the following:

$$\mathrm{tr}(HX^T UU^T XHL) = \mathrm{tr}(U^T XHLHX^T U). \tag{4}$$

The orthogonal transformation matrix, $U$, which maps the data points to a space where features are not correlated, is solved by optimizing the problem which is defined as

$$\arg\max_U \mathrm{tr}(U^T XHLHX^T U), \quad \text{s.t.: } UU^T = 1 \tag{5}$$

where the notation $\arg\max_U$ indicates a maximization problem considering U as an argument. The optimization problem shown in (5) can be solved in closed-form. The symmetric and real matrix $Q = XHLHX^T$ of size $p \times p$, has $p$ number of eigenvalues ($\lambda_1 \leq \cdots \leq \lambda_p$) and corresponding eigenvectors $[\nu_1, \ldots, \nu_p]$, each consisting of $p$ number of elements. In general, the maximum value of the cost function is $\lambda_p + \lambda_{p-1} + \cdots + \lambda_{p-d+1}$ and the optimum solution is $U = [\nu_p, \nu_{p-1}, \ldots, \nu_{p-d+1}]$, where $d$ is the dimension of $[U^T X]$. Since the soil moisture is the only target variable in this paper, the value of $d$ is one, i.e., $[U^T X]$ is a vector of dimension one. Hence, $U = [\nu_p]$, which produces the coefficients for $p$ different input variables and ensures the best association of the product to the output variable.

In this paper, different sets of inputs are considered to find out the effect of any particular input or a subset of the inputs and to select an optimum combination input variables. However, when the number of inputs is more than one, SPCA is applied to derive the combined index of the considered set of inputs reducing the model dimensionality. The square of the SPCA coefficients represents the contribution of each input variable to estimate the target output, and as mentioned earlier, the sum of the square of the SPCA coefficients is equal to one. Therefore, the comparison of the absolute values of the SPCA coefficients corresponding to each specific input helps to select the best possible combination of inputs to develop the combined index to estimate the surface SMC with least model complexity. In addition, it ensures that the selected combination of the input variables has the maximum association with the target variable, i.e., the surface SMC. Using this combined index as an input, probabilistic estimation of SMC is carried out using copula, as explained in Section III-D.

### D. Probabilistic Volumetric Soil Moisture Estimation

Copulas are the functions that combine the marginal distributions of any two or more variables to get the joint probability distribution between the random variables [38]. The use of copula functions in different fields of application has been popularized due to its capability to model the complete dependence structure with a few parameters [39], [40].

The association between the combined index and the reduced variate of SMC is estimated by using Kendall's Tau ($\tau$), which is a rank-based, nonparametric statistical measure. A suitable distribution is fitted to SMC,

TABLE III
PROPERTIES OF THE PRELIMINARY SELECTED BIVARIATE ARCHIMEDEAN COPULA FUNCTIONS

| Name | Copula Function | Generator Function, $\varphi_\theta(t)$ | Parameter of Joint Distribution $(\theta)$ | |
|---|---|---|---|---|
| | | | Range of $\theta$ | $\theta$ = in terms of Kendall Tau |
| **Clayton** | $\left\{\max\left(u^{-\theta}+v^{-\theta}-1,0\right)\right\}^{-1/\theta}$ | $\frac{1}{\theta}\left(t^{-\theta}-1\right)$ | $[-1,\infty)$ excluding 0 | $\frac{2\tau}{1-\tau}$ |
| **Frank** | $-\frac{1}{\theta}\ln\left(1+\frac{\left(e^{-\theta u}-1\right)\left(e^{-\theta v}-1\right)}{e^{-\theta}-1}\right)$ | $-\ln\left(\frac{\left(e^{-\theta t}-1\right)}{e^{-\theta}-1}\right)$ | $(-\infty,\infty)$ | Solve* $\frac{(D_1(-\theta)-1)}{\theta}=\frac{1}{4}(1-\tau)$ for $\theta$[a] |
| **Gumbel-Hougaard** | $\exp\left(-\left\{(-\ln u)^\theta+(-\ln v)^\theta\right\}^{\frac{1}{\theta}}\right)$ | $(-\ln t)^\theta$ | $[1,\infty)$ | $\frac{1}{1-\tau}$ |

[a] $D_1$ is the first –order Debye function, $D_1(\theta)=\frac{1}{\theta}\int_0^\theta \frac{t}{e^t-1}dt$ *for* $\theta>0; D_1(-\theta)=D_1(\theta)+\frac{\theta}{2}$

and the quantile values corresponding to each SMC value are obtained. The quantile values range from 0 to 1 and designated as the "reduced variates." Suppose, $V$ and $Y$ are the reduced variate of the combined index and SMC, respectively. Mathematically, Kendall's Tau can be represented by the following equation:

$$\tau = P[(V_i - V_j)(Y_i - Y_j) > 0] - P[(V_i - V_j)(Y_i - Y_j) < 0] \quad (6)$$

where $i$ and $j$ are any two time steps which are not equal (i.e., $i \neq j$). The dependence parameter of copula is obtained by the estimated $\tau$. The frequently used bivariate Archimedean copulas are Ali–Mikhail–Haq (AMH), Clayton, Frank, and Gumbel–Hougaard (GH). However, the AMH copula is not generally considered, since the range of dependence parameter for this copula is very less $\tau = -0.182$ to 0.333. The details of selected copulas are provided in Table III. Initially, the suitable copulas are selected to model the association between reduced variate of surface SMC and combined index based on the best fit to the observations.

*1) Selection of Best Fit Copula:* The appropriateness of a copula is evaluated statistically by goodness of fit (GOF) tests using: 1) empirical copula; 2) Kendall's transform; and 3) Rosenblatt's transform. The approach of testing using empirical copula was developed in [41], which is based on the null hypothesis $H_0 : C \in C_0$ for a specific copula $C_0$ against $H_1 : C \notin C_0$. The distance between the empirical copula ($C_n$) and parametric estimate ($C_n^\theta$) of $C$, which is obtained under $H_0$, is compared in the tests. The GOF tests are based on the statistic $\sqrt{n}\{C_n(v, y) - C_n^\theta(v, y)\}$, where $v$, $y$, and $n$ are the reduced variates of the combined index, SMC, and the number of observations, respectively. The empirical copula ($C_n$) is defined as

$$C_n(v, y) = \frac{1}{n}\sum_{i=1}^{n} \Im(V \leq v, Y \leq y), \quad v, y \in [0, 1] \quad (7)$$

where $\Im(\bullet)$ is the indicator function that takes a value 1 if the argument $\bullet$ is true and 0 if it is false. The *Crame'r–von Mises* and *Kolmogorov–Smirnov (KS)* statistics are established on the distance explained earlier. The *Crame'r–von Mises* statistics ($S_n$) is a widespread GOF test technique for copula models [41]. The statistic $S_n$ is expressed as

$$S_n = \sum_{1}^{n} \left\{C_n(v, y) - C_n^\theta(v, y)\right\}^2. \quad (8)$$

The KS statistic ($T_n$), which is based on the absolute maximum distance between $C_n$ and $C_n^\theta$, can be is expressed as

$$T_n = \mathrm{Max}_{v,y\in[0,1]}\left|\sqrt{n}\left\{C_n(v, y) - C_n^\theta(v, y)\right\}\right|. \quad (9)$$

The copula function with the minimum value of the above-mentioned statistics implies the best fit copula. The superior statistics is given the emphasis if the best fit copula is different for different test statistics. Genest *et al.* [41] suggested the preference order as ($S_n \succ T_n$) based on their power. The copula showing best fit following these measures is selected and symbolized as $C_b(v, y)$.

*2) Copula-Based Probabilistic Simulation Model:* The joint distribution between the surface SMC and the combined index is modeled using the best fit copula out of the preliminary selected set of Archemedian copulas. The probabilistic assessment of the surface SMC is obtained from the distribution conditioned on the combined index obtained from their joint distribution. The conditional (cumulative) distribution of the volumetric SMC conditioned on the combined index ($M$) can be represented as

$$F_{\mathrm{SM}|M}(\mathrm{SM}|M = m) = \frac{\partial C_b(u, v)}{\partial u}. \quad (10)$$

The 50th quantile value is expressed as the expected value (EV) of the SMC, using the above-mentioned conditional distribution. The range of estimated SMC is represented by the 25th quantile [lower limit (LL)] and 75th quantile [upper limit (UL)], i.e., interquantile range, which reflects the associated uncertainty in SMC estimation. The EV (quantile value at 50%) is used as the estimated SMC values corresponding to the observed SMC values. The interquantile range between these values (75th percentile to 25th percentile) quantifies the associated uncertainty in SMC estimation.

The model performances are also evaluated both during model development and testing periods in terms of CC, Nash–Sutcliffe coefficient (NSE), refined index of agreement (Dr), rms error (RMSE), and unbiased RMSE (uRMSE) [42], [43].

### E. Model Development and Calibration

The available data set is randomly shuffled for 20 times to eliminate any possible bias (for example, the training data set only contains the data from bare or only vegetated land areas) present in the data. The proposed model is developed and tested for each shuffle and the performance is evaluated in terms of the mean of the performances obtained from each shuffle. For each shuffle, the $k$-fold cross-validation technique is used for evaluating the generalized model performance to an independent data set and to avoid over fitting. This cross-validation technique randomly splits a data set into $k$ separate folds with almost identical size, and each fold is in turn used to test the model developed from the remaining $k-1$ folds.

The total number of monitoring points is found to be 334 having the SMC above WP. Among the 334 data points, 32 data points belong to bareland areas and remaining 302 data points belong to vegetated land areas (<30 cm height). For this paper, the data are split into three different folds. The first and second folds contain ten data points from bareland areas and 100 data points from the vegetated land areas, whereas the third fold consists of 12 data points from the bareland areas and 102 points from the vegetated land areas.

The SPCA coefficients corresponding to each input variable and the model performance values for each threefolds are presented in terms of the mean values of 20 shuffles in the result and discussion section. However, in this process, the sum of square of the SPCA coefficients (after taking the mean) could deviate a little from one (in the order of 0.001–0.003). This little deviation, if any, is adjusted mathematically to attain the summation is equal to one.

## IV. Results and Discussion

### A. Selection of Input Variable Combination

Initially, all the seven inputs, i.e., *HH*, *HV*, *VH*, *VV*, %Sand, %Silt, and %Clay, are considered. The sensitivity of each input variable is measured for combined bare and vegetated land areas by computing the SPCA coefficients during model development period. It is observed that the contribution of *HH* is the maximum in surface SMC estimation. This is confirmed by the highest value of absolute value of the coefficients corresponding to *HH,* which ranges from 0.900 to 0.947. Following the averaging and adjustment of the SPCA coefficient values as mentioned earlier, the coefficient corresponding to *HH* is 0.924. Similarly, the absolute values of the coefficients corresponding to *VH* (0.227) and *HV* (0.209) show the second and third highest values, respectively. The absolute values of SPCA coefficients corresponding to remaining input variables, i.e., *VV*, %Sand, %Silt, and %Clay, are 0.126, 0.121, 0.110, and 0.056, respectively. Therefore, to reduce the model complexity, the effect all backscattering coefficients are taken into account by using the radar vegetation index (*RVI*) along with the *HH*. The *RVI* is expressed as the following [44]:

$$RVI = \frac{8\sigma_{HV}}{\sigma_{HH} + \sigma_{VV} + 2\sigma_{HV}}. \tag{11}$$

The range of *RVI* is 0–1. For bareland, the value of *RVI* is near 0 and it increases with the crop growth [44]. Next, using *HH* and *RVI*, a combined index is developed through SPCA. The resulting SPCA coefficients corresponding to *HH* and *RVI*, following the 20 shuffles and modification as mentioned in methodology, are observed to be 0.904 and 0.428, respectively, for the combined bare and vegetated land surfaces. Thus, the contribution of *HH* is still high and the contribution of *RVI* is also significant while avoiding the use of all four backscattering coefficients.

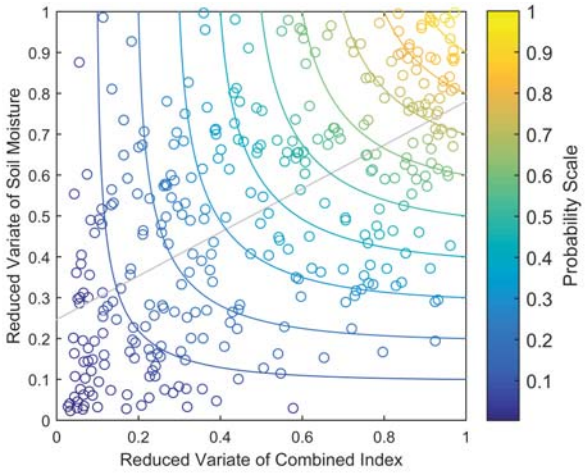


Fig. 1. Scatter plot between the reduced variate of soil moisture and the combined index. The black straight line shows the least square error fit line. The color of data points shows the cdf value and the contour lines show the points having equal values of cdf.

### B. Development of Probabilistic Simulation Model Based on Copula

Using the developed combined index and the observed SMC, best-fit copula is identified to develop the probabilistic simulation model. It has been observed that the values of $S_n$ for Clayton, Frank, and GH copulas are 0.102, 0.086, and 0.133, respectively. The values of $T_n$ for Clayton, Frank, and GH copulas are 14.595, 14.790, and 14.769, respectively. Thus, based on these values, Frank copula is selected to develop the joint distribution between the surface soil moisture and the combined index for combined bare and vegetated land areas.

*1) Joint Distribution Between Combined Index and the Soil Moisture Data:* The marginal distribution of the combined index is investigated to follow the normal distribution, and the observed SMC above WP is fitted to empirical distribution as its best fit probability distribution. The joint distribution of the SMC and the combined index is modeled using Frank copula. The dependence parameter ($\theta$) for the joint distribution is attained from the Kendall's tau ($\tau$) between the observed SMC and developed combined index. Kendall's tau between the observed SMC and combined index is found to be 0.394 for combined vegetated and bareland areas. The dependence parameter of the Frank copula, $\theta$, is found to be 4.084. In Fig. 1, the cumulative distribution function (cdf) of the Frank copula is superimposed on the scatter plots between the reduced variates of soil moisture and the inputs. From Fig. 1, it can be seen that the cdf of the selected Frank copula fits

TABLE IV

COMPARISON OF PERFORMANCE METRICS OF THE MODEL FOR ALL THREEFOLDS WITH ALL THE SEVEN ($HH$, $HV$, $VH$, $VV$, %SAND, %SILT, AND %CLAY) INPUT COMBINATION

| Performance Metrics | | Fold 1 | | | Fold 2 | | | Fold 3 | | |
|---|---|---|---|---|---|---|---|---|---|---|
| | | Min | Max | Mean | Min | Max | Mean | Min | Max | Mean |
| CC | Dev | 0.527 | 0.624 | 0.569 | 0.496 | 0.601 | 0.556 | 0.509 | 0.617 | 0.563 |
| | Test | 0.364 | 0.633 | 0.541 | 0.490 | 0.651 | 0.564 | 0.457 | 0.671 | 0.546 |
| Dr | Dev | 0.602 | 0.634 | 0.616 | 0.586 | 0.630 | 0.611 | 0.598 | 0.638 | 0.614 |
| | Test | 0.558 | 0.638 | 0.601 | 0.570 | 0.647 | 0.610 | 0.537 | 0.649 | 0.603 |
| NSE | Dev | 0.267 | 0.382 | 0.315 | 0.237 | 0.355 | 0.301 | 0.253 | 0.371 | 0.309 |
| | Test | 0.064 | 0.397 | 0.270 | 0.219 | 0.406 | 0.300 | 0.171 | 0.422 | 0.276 |
| RMSE | Dev | 0.088 | 0.102 | 0.094 | 0.086 | 0.102 | 0.095 | 0.085 | 0.102 | 0.093 |
| | Test | 0.076 | 0.108 | 0.095 | 0.076 | 0.114 | 0.093 | 0.085 | 0.114 | 0.098 |
| uRMSE | Dev | 0.088 | 0.102 | 0.094 | 0.086 | 0.101 | 0.095 | 0.085 | 0.101 | 0.093 |
| | Test | 0.076 | 0.107 | 0.095 | 0.076 | 0.111 | 0.093 | 0.084 | 0.111 | 0.097 |

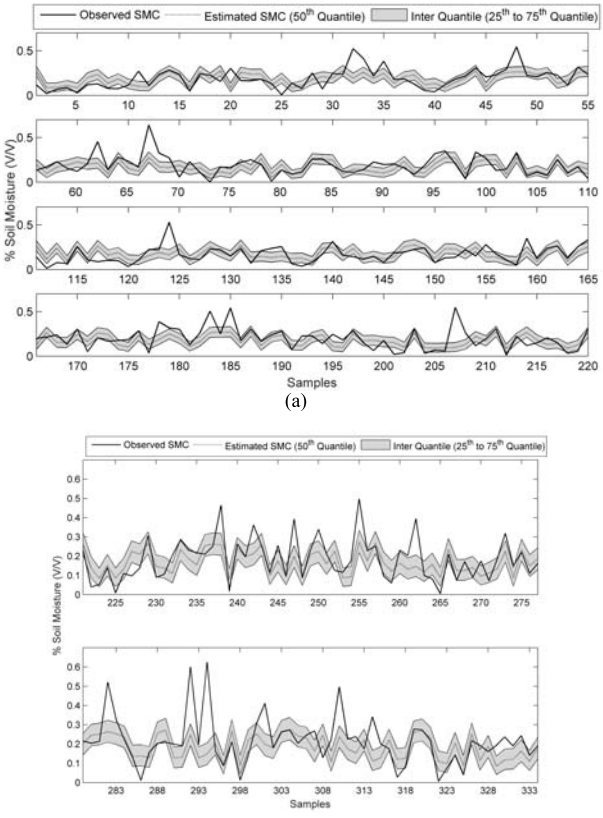


Fig. 2. Comparison of the estimated and observed soil moisture with the uncertainty range during (a) model development period and (b) model testing period.

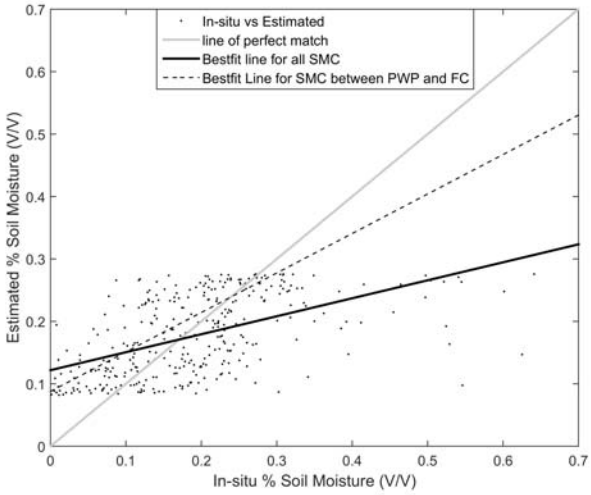


Fig. 3. Scatter plot between the estimated and observed soil moisture with the best fit line for the SMC between PWP and FC.

proficiently with the distribution of the reduced variates of the SMC and the combined input variables.

The conditional distribution of SMC, conditioned on combined index using (10), is attained by using the developed joint distribution. The conditional cumulative distribution is used to calculate the quantile values at 25%, 50%, and 75% probability and used as the LL, EV, and UL of the estimated SMC, respectively. Fig. 2 shows the comparison between the estimated SMC and the observed SMC with their uncertainty range. Fig. 3 shows the scatter plot between the observed and the estimated SMC for the entire range of SMC available for the study area.

For the present study area, the range of permanent WP (PWP) to field capacity (FC) has been computed for combined bare and vegetated land areas to be 4.73%–32.93%. The comparison between line of perfect match and best fit line with all SMC shows relatively poor model performance. However, the comparison between the line of perfect match and best fit line for SMC between the PWP and FC shows that the discrepancy decreases drastically. It can be observed from Fig. 3 that the proposed model performs better in the specific range between the PWP and the FC.

*2) Model Performance:* The performance of the model is assessed in terms of CC, NSE, Dr, RMSE, and uRMSE for randomly shuffled data as mentioned earlier for each fold. Therefore, the model performances are compared between different folds for different shuffles, and the mean values along with the maximum and minimum values are reported to assess the performance of the proposed approach.

Table IV represents the minimum, maximum, and mean values of the considered performance metrics of all the

TABLE V
COMPARISON OF PERFORMANCE METRICS OF THE MODEL FOR ALL THREEFOLDS CONSIDERING *H H* AND *RVI* AS THE INPUT COMBINATION

| Performance Metrics | | Fold 1 | | | Fold 2 | | | Fold 3 | | |
|---|---|---|---|---|---|---|---|---|---|---|
| | | Min | Max | Mean | Min | Max | Mean | Min | Max | Mean |
| CC | Dev | 0.492 | 0.625 | 0.528 | 0.471 | 0.549 | 0.514 | 0.456 | 0.555 | 0.522 |
| | Test | 0.310 | 0.584 | 0.498 | 0.438 | 0.617 | 0.540 | 0.435 | 0.660 | 0.516 |
| Dr | Dev | 0.578 | 0.617 | 0.589 | 0.572 | 0.604 | 0.584 | 0.568 | 0.599 | 0.587 |
| | Test | 0.497 | 0.601 | 0.571 | 0.533 | 0.615 | 0.589 | 0.541 | 0.628 | 0.581 |
| NSE | Dev | 0.228 | 0.381 | 0.269 | 0.209 | 0.293 | 0.253 | 0.198 | 0.303 | 0.263 |
| | Test | -0.062 | 0.328 | 0.218 | 0.151 | 0.371 | 0.268 | 0.166 | 0.407 | 0.246 |
| RMSE | Dev | 0.090 | 0.108 | 0.097 | 0.089 | 0.105 | 0.098 | 0.088 | 0.104 | 0.096 |
| | Test | 0.076 | 0.115 | 0.099 | 0.077 | 0.113 | 0.095 | 0.085 | 0.115 | 0.100 |
| uRMSE | Dev | 0.089 | 0.107 | 0.097 | 0.089 | 0.104 | 0.098 | 0.088 | 0.104 | 0.096 |
| | Test | 0.076 | 0.114 | 0.098 | 0.077 | 0.111 | 0.094 | 0.085 | 0.112 | 0.099 |

20 shuffles for the threefolds, while all the seven input variables are considered. It has been observed that the values of the mean of the CC, Dr, NSE, RMSE, and uRMSE are 0.569, 0.616, 0.315, 0.094, and 0.094, respectively, for the first fold which is better compared with second and third folds during the development period. However, during the testing period, the mean values of the performance metrics are marginally higher for the second fold (CC-0.564, Dr-0.610, NSE-0.300, RMSE-0.093, and uRMSE-0.093) than the first and third folds. Table V shows the minimum, maximum, and mean values of the performance metrics for all the 20 shuffles and threefolds both during the development and testing period using the combined index of *HH* and *RVI*. It is observed that the mean values of CC, Dr, NSE, RMSE, and uRMSE are found to be 0.528, 0.589, 0.269, 0.097, and 0.097, respectively, for the first fold during the development period.

Similarly, the mean values of the above-mentioned performance metrics are 0.514, 0.584, 0.253, 0.098, and 0.098 for the second fold and 0.522, 0.587, 0.263, 0.096, and 0.096 for the third fold. Thus, the mean values of the performance metrics are almost comparable for each threefolds during the development periods. However, during the testing period, the mean values of the performance metrics are found to be best for the second fold. Following the comparison of the performance metrics values for all the threefolds during both development and testing period, it can be concluded that the moderately high values of CC, Dr, and NSE and low values of RMSE and uRMSE show a good association between the estimated SMC with the observed SMC for combined bare and vegetated land areas. Furthermore, while applying the model for two different dates (two different incident angles) separately, it is noticed that there is not much change in the performance except some statistical randomness. Thus, the normalization of the incidence angle enables the model to be applied uniformly for two different incidence angles.

The comparison between Tables IV and V show that the use of the combined index considering both the *HH* and *RVI* by merging the radar signal data is effective to estimate the surface SMC for combined bare and vegetated land surfaces (<30 cm height). In addition, it also suggests that indeed the inclusion of soil texture information enhances the model performance for both the development and testing periods to some extent. To investigate whether the model performance is acceptable for the cases with and without soil texture information, the 5% significance level of CC (95% confidence interval) region is explored for training and testing period. It is found to be $\pm 0.132$ for training period. The values of the CC for the threefolds are outside this range, for both the cases with and without the soil texture information, which are 0.556–0.569 and 0.541–0.564, respectively. For testing period, 95% confidence interval of CC is $\pm 0.184$. Again, it is observed that the values of the CC for both cases are not within the significance level of CC during the testing period, which are 0.514–0.528 and 0.498–0.540 for with and without the soil texture information, respectively. Therefore, it can be concluded that model performance is acceptable for both the cases with and without soil texture information. Since soil texture information may not be readily available for all locations, the model without the soil texture information can be adopted at the cost of a little compromise on the model performance but with a wide scope of applicability. It increases the scope of spatial transferability of the model toward the generation of soil moisture map using *HH* and *RVI*.

### C. Soil Moisture Map

Using the proposed approach, we are able to apply the ancillary data sets of RISAT1 for each date on a pixel by pixel basis to develop soil moisture map. However, since the model applicability is limited to the bare and vegetated land areas (<30 cm), the pixels, which cannot be categorized in either of these two classes, were identified and tagged as inapplicable zones. For rest of the regions, the soil moisture maps are obtained without the soil texture information in the input data set. The resulting soil moisture maps are shown in Figs. 4 and 5 for October 25, and October 27, 2014, respectively. The yellow is the indicative of low soil moisture and the blues indicate high soil moisture. The white patches indicate the inapplicable zones (i.e., establishments or with vegetation height more than 30 cm). Such a map derived from remotely sensed data may be of immense use in different fields

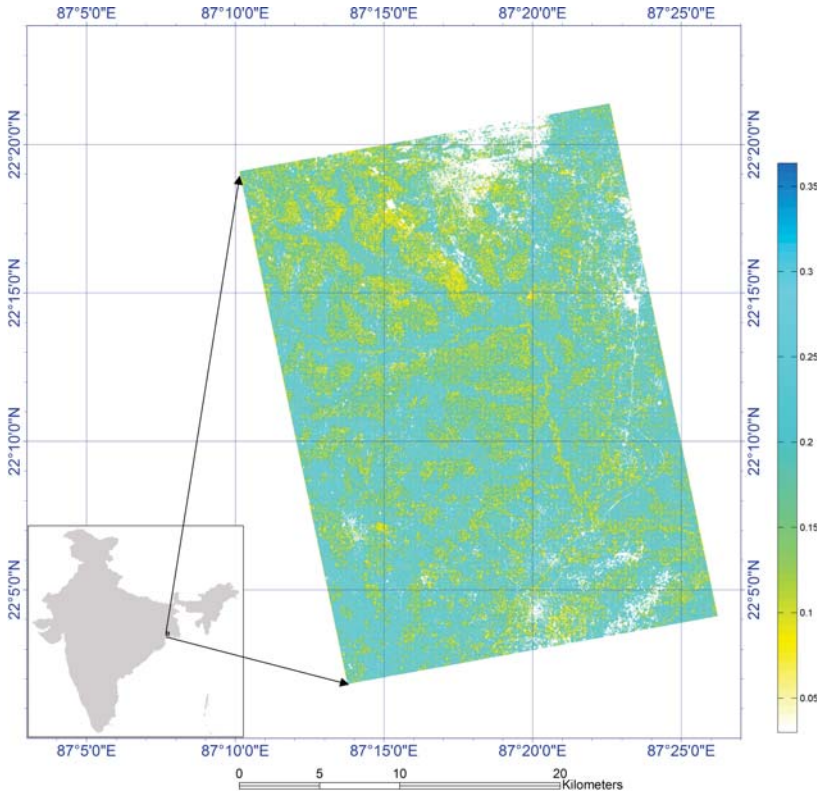


Fig. 4. Soil moisture (above WP) map of October 25, 2014. The soil moisture is represented in volumetric term ($m^3/m^3$).

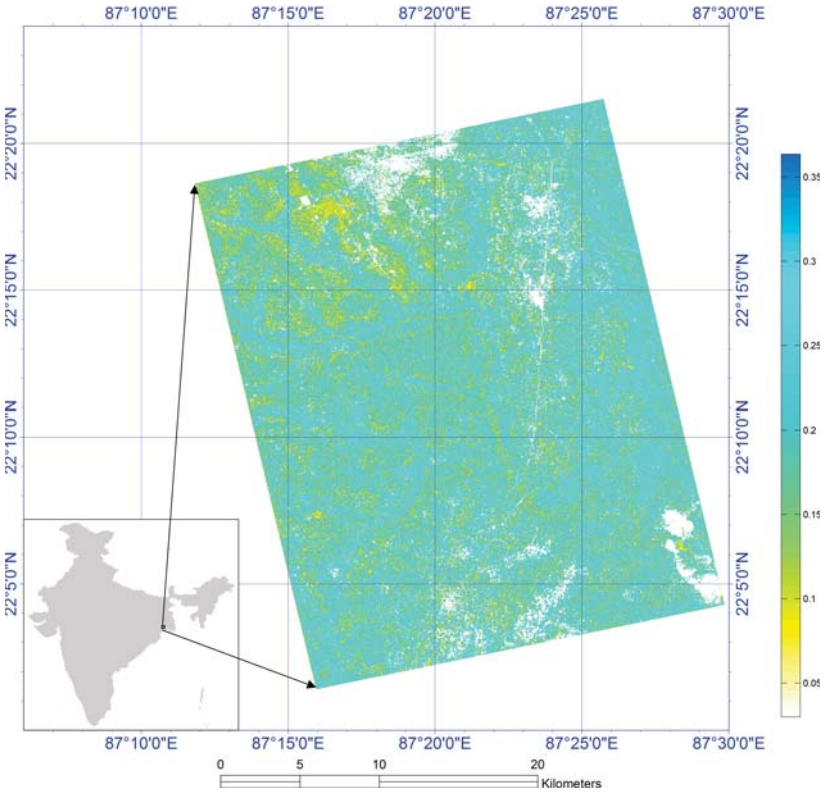


Fig. 5. Soil moisture (above WP) map of October 27, 2014. The soil moisture is represented in volumetric term ($m^3/m^3$).

of application. However, it is worthwhile to reiterate one issue that such map provides soil moisture information only from top surface (<10 cm), which is common issue for microwave remote sensing data. Estimation of SMC for deeper layer using the information top surface may be considered as a further scope of this paper.

## V. Conclusion

The research gaps motivate this paper to develop a non-site specific model for estimating the surface SMC using quad-polarized microwave remote sensing data (RISAT1). The developed model is spatially transferable and able to develop soil moisture map irrespective of surface roughness and incidence angle. Detailed information on LULC is also not required if it is either bare or vegetation height within 30 cm.

This paper introduces a model based on copula and it applies the incidence angle normalization to enable the model to be used for different incidence angles. The SPCA method used to select an ideal combination of possibly influencing input variables for optimum model complexity leads to the conclusion that *HH* is having the highest association with the surface SMC above WP. A decent contribution of cross-polarized backscattering coefficients (*HV* and *VH*) for estimating the output is also indicated through SPCA analysis. Therefore, to incorporate the effects of all the backscattering coefficients, *RVI* is computed, and it is shown that *RVI* and *HH* are sufficient to obtain the combined index to serve as an effective input for SMC estimation. The mean values of CC, Dr, and NSE in all the threefolds ranging from 0.514–0.528, 0.584–0.589, and 0.253–0.269, respectively, and the values of RMSE and uRMSE both ranging from 0.096–0.098 conform the stated good performance of the model for combined bare-land and vegetated land areas during the model development period using *HH* and *RVI*. During the testing period, the values of CC, Dr, NSE, RMSE, and uRMSE (0.498–0.540, 0.571–0.589, 0.218–0.268, 0.096–0.098, and 0.094–0.099, respectively) deteriorate, yet it is reasonably acceptable given the complexity of the model. Another novelty of the developed copula-based approach is the uncertainty quantification with reasonably acceptable model performance. Hence, it can be said that the findings of this paper are expected to have a wide range applications and studies.

## Appendix
## Determining the Field Capacity and Permanent Wilting Point

The soil–water characteristic equation is described as the following [45]:

$$\psi = A\theta^B \tag{A1}$$

where $\psi$ = Soil water potential expressed in Bar, $\theta$ is the SMC at that soil moisture potential, and $A$ and $B$ are the coefficients computed with the percentage of sand and clay information. The computation of A and B is described as follows:

$$\ln(A) = a + b(\%\text{Clay}) + c(\%\text{sand})^2 + d(\%\text{Sand})^2(\%\text{Clay}) \tag{A2}$$

$$B = e + f(\%\text{Clay})^2 + g(\%\text{Sand})^2 + g(\%\text{Sand})^2(\%\text{Clay}). \tag{A3}$$

The values of the coefficients are provided as the following:

$$a = -4.396 \quad b = -0.0715 \quad c = -4.880 \times 10^{-4}$$
$$d = -4.285 \times 10^{-5} \quad e = -3.140 \quad f = -2.22 \times 10^{-3}$$
$$g = -3.484 \times 10^{-5}.$$

The SMC at WP and FC is defined as the SMC at 15 bar and 0.3333 bar suction pressure, respectively. Therefore, using (A1), the SMC at 15 bar, and 0.3333 bar suction pressure, the WP and the FC are computed.

## References


[1] G. C. Heathman, P. J. Starks, and M. A. Brown, "Time domain reflectometry field calibration in the little Washita River experimental watershed," *Soil Sci. Soc. Amer. J.*, vol. 67, no. 1, pp. 52–61, 2003.

[2] F. T. Ulaby, R. K. Moore, A. K. Fung, and F. T. Ulaby, *Microwave Remote Sensing: Active and Passive*, vol. 2. Reading, MA, USA: Addison-Wesley, 1982.

[3] H. S. Srivastava, P. Patel, Y. Sharma, and R. R. Navalgund, "Large-area soil moisture estimation using multi-incidence-angle RADARSAT-1 SAR data," *IEEE Trans. Geosci. Remote Sens.*, vol. 47, no. 8, pp. 2528–2535, Aug. 2009.

[4] R. Hoeben and P. A. Troch, "Assimilation of active microwave observation data for soil moisture profile estimation," *Water Resour. Res.*, vol. 36, no. 10, pp. 2805–2819, Oct. 2000.

[5] M. W. J. Davidson, T. L. Toan, F. Mattia, G. Satalino, T. Manninen, and M. Borgeaud, "On the characterization of agricultural soil roughness for radar remote sensing studies," *IEEE Trans. Geosci. Remote Sens.*, vol. 38, no. 2, pp. 630–640, Mar. 2000.

[6] G. Satalino, F. Mattia, M. W. J. Davidson, T. L. Toan, G. Pasquariello, and M. Borgeaud, "On current limits of soil moisture retrieval from ERS-SAR data," *IEEE Trans. Geosci. Remote Sens.*, vol. 40, no. 11, pp. 2438–2447, Nov. 2002.

[7] F. Mattia *et al.*, "A comparison between soil roughness statistics used in surface scattering models derived from mechanical and laser profilers," *IEEE Trans. Geosci. Remote Sens.*, vol. 41, no. 7, pp. 1659–1671, Jul. 2003.

[8] J. Alvarez-Mozos, J. Casali, M. Gonzalez-Audicana, and N. E. C. Verhoest, "Assessment of the operational applicability of RADARSAT-1 data for surface soil moisture estimation," *IEEE Trans. Geosci. Remote Sens.*, vol. 44, no. 4, pp. 913–924, Apr. 2006.

[9] H. S. Srivastava, P. Patel, M. L. Manchanda, and S. Adiga, "Use of multiincidence angle RADARSAT-1 SAR data to incorporate the effect of surface roughness in soil moisture estimation," *IEEE Trans. Geosci. Remote Sens.*, vol. 41, no. 7, pp. 1638–1640, Jul. 2003.

[10] W. Wagner *et al.*, "Operational readiness of microwave remote sensing of soil moisture for hydrologic applications," *Hydrol. Res.*, vol. 38, no. 1, pp. 1–20, 2007.

[11] A. Merzouki, H. McNairn, and A. Pacheco, "Mapping soil moisture using RADARSAT-2 data and local autocorrelation statistics," *IEEE J. Sel. Topics Appl. Earth Observ. Remote Sens.*, vol. 4, no. 1, pp. 128–137, Mar. 2011.

[12] G. Macelloni *et al.*, "The SIR-C/X-SAR experiment on Montespertoli: Sensitivity to hydrological parameters," *Int. J. Remote Sens.*, vol. 20, no. 13, pp. 2597–2612, Jan. 1999.

[13] S. Paloscia, G. Macelloni, P. Pampaloni, and E. Santi, "The contribution of multitemporal SAR data in assessing hydrological parameters," *IEEE Geosci. Remote Sens. Lett.*, vol. 1, no. 3, pp. 201–205, Jul. 2004.

[14] N. Pierdicca, L. Pulvirenti, and C. Bignami, "Soil moisture estimation over vegetated terrains using multitemporal remote sensing data," *Remote Sens. Environ.*, vol. 114, no. 2, pp. 440–448, Feb. 2010.

[15] A. Balenzano, G. Satalino, V. Pauwels, and F. Mattia, "Soil moisture retrieval from dense temporal series of C-band SAR data over agricultural sites," in *Proc. IEEE Int. Geosci. Remote Sens. Symp. (IGARSS)*, Jul. 2011, pp. 3136–3139.

[16] M. Doubková, A. I. J. M. Van Dijk, D. Sabel, W. Wagner, and G. Blöschl, "Evaluation of the predicted error of the soil moisture retrieval from C-band SAR by comparison against modelled soil moisture estimates over Australia," *Remote Sens. Environ.*, vol. 120, pp. 188–196, May 2012.

[17] R. van der Velde, Z. Su, P. van Oevelen, J. Wen, Y. Ma, and M. S. Salama, "Soil moisture mapping over the central part of the Tibetan Plateau using a series of ASAR WS images," *Remote Sens. Environ.*, vol. 120, pp. 175–187, May 2012.

[18] P. C. Dubois, J. V. Zyl, and T. Engman, "Measuring soil moisture with imaging radars," *IEEE Trans. Geosci. Remote Sens.*, vol. 33, no. 4, pp. 915–926, Jul. 1995.

[19] J. Shi, J. Wang, A. Y. Hsu, P. E. O'Neill, and E. T. Engman, "Estimation of bare surface soil moisture and surface roughness parameter using L-band SAR image data," *IEEE Trans. Geosci. Remote Sens.*, vol. 35, no. 5, pp. 1254–1266, Sep. 1997.

[20] Y. Oh, K. Sarabandi, and F. T. Ulaby, "Semi-empirical model of the ensemble-averaged differential Mueller matrix for microwave backscattering from bare soil surfaces," *IEEE Trans. Geosci. Remote Sens.*, vol. 40, no. 6, pp. 1348–1355, Jun. 2002.

[21] T.-D. Wu and K.-S. Chen, "A reappraisal of the validity of the IEM model for backscattering from rough surfaces," *IEEE Trans. Geosci. Remote Sens.*, vol. 42, no. 4, pp. 743–753, Apr. 2004.

[22] F. T. Ulaby, R. K. Moore, A. K. Fung, and F. T. Ulaby, *Microwave Remote Sensing: Active and Passive*, vol. 3. Reading, MA, USA: Addison-Wesley, 1986.

[23] K. C. Kornelsen and P. Coulibaly, "Advances in soil moisture retrieval from synthetic aperture radar and hydrological applications," *J. Hydrol.*, vol. 476, pp. 460–489, Jan. 2013.

[24] A. K. Fung, Z. Li, and K. S. Chen, "Backscattering from a randomly rough dielectric surface," *IEEE Trans. Geosci. Remote Sens.*, vol. 30, no. 2, pp. 356–369, Mar. 1992.

[25] J. P. Wigneron *et al.*, "Characterizing the dependence of vegetation model parameters on crop structure, incidence angle, and polarization at L-band," *IEEE Trans. Geosci. Remote Sens.*, vol. 42, no. 2, pp. 416–425, Feb. 2004.

[26] GSOC, "Implementation plan for the global observing system for climate in support of the UNFCCC (2010 update)," World Meteorol. Org., Geneva, Switzerland, Tech. Rep. GCOS-138, 2010.

[27] S. Paloscia, S. Pettinato, E. Santi, C. Notarnicola, L. Pasolli, and A. Reppucci, "Soil moisture mapping using Sentinel-1 images: Algorithm and preliminary validation," *Remote Sens. Environ.*, vol. 134, pp. 234–248, Jul. 2013.

[28] W. A. Dorigo *et al.*, "Evaluation of the ESA CCI soil moisture product using ground-based observations," *Remote Sens. Environ.*, vol. 162, pp. 380–395, Jun. 2015.

[29] H. S. Srivastava, P. Patel, and R. R. Navalgund, "Incorporating soil texture in soil moisture estimation from extended low-1 beam mode RADARSAT-1 SAR data," *Int. J. Remote Sens.*, vol. 27, no. 12, pp. 2587–2598, Jun. 2006.

[30] Indian Standards, *Methods of Test for Soils, Part 3: Determination of Specific Gravity, Section 1: Fine Grained Soils [CED 43: Soil and Foundation Engineering]*, document IS 2720-3-1, Bureau of Indian Standards, New Delhi, India, 1980.

[31] Indian Standards, *Methods of Test for Soils, Part 4: Grain Size Analysis [CED 43: Soil and Foundation Engineering]*, document IS 2720-4, Bureau of Indian Standards, New Delhi, India, 1985.

[32] M. D. Mishra, P. Patel, H. S. Srivastava, P. R. Patel, A. Shukla, and A. K. Shukla, "Absolute radiometric calibration of FRS-1 and MRS mode of RISAT-1 synthetic aperture radar (SAR) data using corner reflectors," *Internat. J. Adv. Eng. Res. Sci.*, vol. 1, no. 6, pp. 78–89, Nov. 2014.

[33] M. Zribi, N. Baghdadi, N. Holah, and O. Fafin, "New methodology for soil surface moisture estimation and its application to ENVISAT-ASAR multi-incidence data inversion," *Remote Sens. Environ.*, vol. 96, nos. 3–4, pp. 485–496, Jun. 2005.

[34] A. K. Fung and M. F. Chen, "Numerical simulation of scattering from simple and composite random surfaces," *J. Opt. Soc. Amer. A*, vol. 2, no. 12, pp. 2274–2284, 1985.

[35] E. Barshan, A. Ghodsi, Z. Azimifar, and M. Z. Jahromi, "Supervised principal component analysis: Visualization, classification and regression on subspaces and submanifolds," *Pattern Recognit.*, vol. 44, no. 7, pp. 1357–1371, Jul. 2011.

[36] A. Gretton, O. Bousquet, A. Smola, and B. Schölkopf, "Measuring statistical dependence with Hilbert–Schmidt norms," in *Algorithmic Learning Theory*, vol. 3734, S. Jain, H. U. Simon, and E. Tomita, Eds. Berlin, Germany: Springer, 2005, pp. 63–77.

[37] N. Aronszajn, "Theory of reproducing kernels," *Trans. Amer. Math. Soc.*, vol. 68, no. 3, pp. 337–404, 1950.

[38] R. B. Nelsen, *An Introduction to Copulas*, 2nd ed. New York, NY, USA: Springer, 2010, p. 269.

[39] M. Gebremichael and W. F. Krajewski, "Application of copulas to modeling temporal sampling errors in satellite-derived rainfall estimates," *J. Hydrol. Eng.*, vol. 12, no. 4, pp. 404–408, Jul. 2007.

[40] R. Maity and D. N. Kumar, "Probabilistic prediction of hydroclimatic variables with nonparametric quantification of uncertainty," *J. Geophys. Res.*, vol. 113, no. (D14), D14105, pp. 1–12, Jul. 2008.

[41] C. Genest, B. Rémillard, and D. Beaudoin, "Goodness-of-fit tests for copulas: A review and a power study," *Insurance Math. Econ.*, vol. 44, no. 2, pp. 199–213, Apr. 2009.

[42] P. Krause, D. P. Boyle, and F. Bäse, "Comparison of different efficiency criteria for hydrological model assessment," *Adv. Geosci.*, vol. 5, pp. 89–97, Dec. 2005.

[43] C. J. Willmott, S. M. Robeson, and K. Matsuura, "A refined index of model performance," *Int. J. Climatol.*, vol. 32, no. 13, pp. 2088–2094, Nov. 2012.

[44] Y. Kim, T. Jackson, R. Bindlish, H. Lee, and S. Hong, "Radar vegetation index for estimating the vegetation water content of rice and soybean," *IEEE Geosci. Remote Sens. Lett.*, vol. 9, no. 4, pp. 564–568, Jul. 2012.

[45] K. E. Saxton, W. J. Rawls, J. S. Romberger, and R. I. Papendick, "Estimating generalized soil-water characteristics from texture," *Soil Sci. Soc. Amer. J.*, vol. 50, no. 4, pp. 1031–1036, 1986.

**Manali Pal** received the B.Tech. degree in Agricultural Engineering from Uttar Banga Krishi Vishwavidyalaya, Cooch Behar, India, in 2010, and the M.Tech. degree in Earth System Science and Technology from IIT Kharagpur, Kharagpur, India, in 2013, where she is currently pursuing the Ph.D. degree with the School of Water Resources.

Her current research interests include hydrology, remote sensing, climate change, estimation of soil moisture from remote sensing data, and stochastic modeling of vertical soil moisture profile.

**Rajib Maity** received the M.E. degree (Gold Medallist) and the Ph.D. degree from the Indian Institute of Science (IISc), Bangalore, India, in 2004 and 2007, respectively.

He is currently an Associate Professor with the Civil Engineering Department, IIT Kharagpur, Kharagpur, India, and a Guest Scientist (Humboldt Fellow) with the Karlsruhe Institute of Technology, Campus Alpin-IMK-IFU, Garmisch-Partenkirchen, Germany. He has authored one book and over 75 research articles in different peer-reviewed journals and conferences and chapters in books. His current research interests include hydroclimatology, climate impacts on water resources, stochastic hydrology, and hydrologic applications of satellite remote sensing.

Dr. Maity was a recipient of the Prof. R. J. Garde Research Award, the IEI Young Engineers Award, and the Prof. N. S. Govinda Rao Memorial Gold Medal, IISc. He received the ASCE 2011 Outstanding Reviewer, USA, the Emerging Leaders Fellowship, Australia, the BOYSCAST Fellowship, the DAAD Fellowship for IIT Faculty, Germany, the International ICE WaRM Fellowship, Australia, and the Humboldt Research Fellowship for Experienced Researchers by Alexander von Humboldt Foundation, Germany. He serves as an Associate Editor of the *Journal of Earth System Sciences* (Springer), and the *ISH Journal of Hydraulic Engineering*, published by Taylor and Francis.

**Mayank Suman** received the B.Tech. degree in Civil Engineering from the National Institute of Technology, Hamirpur, India, in 2013, and the M.Tech. degree in Hydraulics and Water Resources from IIT Kharagpur, Kharagpur, India, in 2015, where he is currently pursuing the Ph.D. degree with the School of Water Resources.

He is currently a Research Scholar with IIT Kharagpur. His current research interests include hydroclimatology, specially the effect of climate change on the hydrological extremes, statistical analysis of hydrological time series, and application of wavelet transformation and copula theory in hydroclimatic analysis.

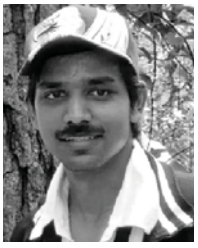

**Sarit Kumar Das** was born in Howrah, India. He received the B.E. degree in Civil Engineering from the Indian Institute of Engineering Science and Technology at Shibpur, Howrah, in 2004, the M.Tech. degree in Environmental Science and Engineering from IIT Bombay, Mumbai, India, in 2007, the M.S. degree in Environmental Engineering from the University of New Orleans, New Orleans, LA, USA, in 2009, and the Ph.D. degree in civil engineering from IIT Kharagpur, Kharagpur, India, in 2015.

In 2016, he joined the National Institute of Technology Sikkim, Ravangla, India, as an Assistant Professor, and subsequently joined IIT Roorkee, Roorkee, India, as a DST-INSPIRE Faculty, where he is currently with the Hydraulics Section, Civil Engineering Department. His current research interests include probabilistic simulation techniques to model the soil moisture feedback into the air pollution meteorology considering geophysical processes inside the planetary boundary layer.

Dr. Das is a member of the American Geophysical Union. He received the INSPIRE Faculty Award from the Department of Science and Technology, Government of India, in 2016.

**Parul Patel** received the M.Sc. degree in Statistics from the Maharaja Sayajirao University of Baroda, Vadodara, India, in 1985, and the Ph.D. degree in Science on Target Parameter Retrieval Using Synthetic Aperture Radar Polarimetry from Nirma University, Ahmedabad, India.

She joined the Space Applications Center (SAC), Indian Space Research Organization (ISRO), Ahmedabad, India, in 1988, where she has been involved in microwave remote sensing activities of SAC. She has carried out a number of investigative studies on target interaction using multiparametric SAR, InSAR, PolSAR, and PolInSAR data from ground-based to space borne sensors, such as ISRO-ground-based scatterometer, ISRO-SLAR, ISRO-ASAR, ERS-1, ERS-2, SIR-B, SIR-C/X-SAR, Intera-X-SAR, DLR-ESAR, JERS-1, RADARSAT-1, RADARSAT-2, RISAT-1, and passive AMSR-E & SMOS. She has contributed significantly in calibration of RISAT-1, ISRO-DMSAR, ERS-1, and ERS-2. She was the Principal Investigator for the European Space Agency's SMOS Cal/Val Announcement of Opportunity and the Canadian Space Agency's RADARSAT-2 Announcement of Opportunity. At present, she looks after the research and development activities of SAC and sponsored research at academia across India. She is currently a Senior Scientist with SAC, ISRO, and a Ph.D. Guide with IIT Dhanbad, Dhanbad, India, and Nirma University. She has authored over 100 research publications.

Dr. Patel is a Reviewer of the IEEE TRANSACTIONS ON GEOSCIENCE AND REMOTE SENSING, the IEEE sc Geoscience and Remote Sensing Letters *Remote Sensing of Environment*, and the *Journal of Applied Remote Sensing*.

**Hari Shanker Srivastava** received the M.Sc. degree (Gold medalist) in Physics from Kanpur University, Kanpur, India, in 1990, and the Ph.D. degree in Physics from the Chhatrapati Shahu Ji Maharaj University, Kanpur, with the focus on synthetic aperture radar (SAR).

He joined Space Applications Centre (SAC), Indian Space Research Organization (ISRO), Ahmedabad, India, in 1991. Since the past 25 years, he has contributed significantly in various microwave remote sensing projects on soil moisture estimation, agricultural studies, crop yield estimation, wetland, forestry, human settlement, InSAR, PolSAR, PolInSAR, and absolute radiometric calibration/validation of ERS-1, ERS-2, and RISAT-1 SAR using multiparametric microwave data from ground-based scatterometer, ISRO airborne SAR, ERS-1 SAR, ERS-1/2 tandem mission, L-band JERS-1 SAR, X-C-L SIR-C/X-SAR, RADARSAT-1 SAR, ENVISAT-1 ASAR, RADARSAT-2 PolSAR, C-L-P fully polarimetric DLR E-SAR, hybrid polarimetric RISAT-1 SAR, and passive AMSR-E and SMOS. He was a Co-Principal Investigator for the European Space Agency's SMOS Cal/Val Announcement of Opportunity (AO) Project and the Canadian Space Agency's RADARSAT-2 (SOAR) AO project. He is currently a Senior Faculty with the Indian Institute of Remote Sensing, Dehradun, India, and also a Faculty of ISRO's EDUSAT-Based Distance Learning Program. He has authored over 100 research publications.

Dr. Srivastava is a Reviewer for various journals, such as the IEEE TRANSACTIONS ON GEOSCIENCE AND REMOTE SENSING, the IEEE GEOSCIENCE AND REMOTE SENSING LETTERS, *Remote Sensing of Environment*, and the *International Journal of Remote Sensing*. He has guided a number of M.Tech. and M.Sc. students in microwave remote sensing applications and currently guiding three Ph.D. students registered with IIT Roorkee, Roorkee, India and IIT Dhanbad, Dhanbad, India.